Technical Paper Series

780416

Experimental and Theoretical Analysis of Wankel Engine Performance

Guido A. Danieli
Dipartimento di Meccanice,
Universita degli Studi della Calabria
Arcavacata di Rende (Cosenza)

James C. Keck and John B. Heywood
Mechanical Engrg. Dept.,
Massachusetts Institute of Technology
Cambridge, MA

Congress and Exposition
Cobo Hall, Detroit
February 27-March 3, 1978

Society of Automotive Engineers

SOCIETY OF AUTOMOTIVE ENGINEERS, INC.
400 COMMONWEALTH DRIVE
WARRENDALE, PENNSYLVANIA 15096

780416

Experimental and Theoretical Analysis of Wankel Engine Performance

Guido A. Danieli
Dipartimento di Meccanice,
Universita degli Studi della Calabria
Arcavacata di Rende (Cosenza)

James C. Keck and John B. Heywood
Mechanical Engrg. Dept.,
Massachusetts Institute of Technology
Cambridge, MA

ABSTRACT

A model for predicting the performance and emissions characteristics of Wankel engines has been developed and tested. Each chamber is treated as an open thermodynamic system and the effects of turbulent flame propagation, quench layer formation, gas motion, heat transfer and seal leakage are included. The experimental tests were carried out on a Toyo Kogyo 12B engine under both motoring and firing conditions and values for the effective seal leakage area and turbulent heat transfer coefficient were deduced. The agreement between the predicted and measured performances was reasonable. Parametric studies of the effects of reductions in seal leakage and heat transfer were carried out and the results are presented.

THE NEED FOR a complete performance model of a Wankel engine, able to take into account the effects of leakage, quenching, heat losses and geometrical constraints on engine power and efficiency has long been recognized. Previous modelling studies of the Wankel by Bracco and Sirignano (1),* by Eberle and Klomp (2), and Danieli et al (3) have been more limited in scope or have had different goals. In the current study, a complete performance model which includes combustion, heat transfer, gas leakage and basic engine geometry has been developed.

Each of the three chambers in a single engine rotor housing is treated as an open thermodynamic system. Different subsystems within the main system were used to seperate unburned, burned and quenched gases from one another. These subsystems were allowed to exchange mass, heat and work between each other as well as with the environment. The energy conservation equation, the mass conservation equation and the perfect gas law are applied to each system. Approximations to real gas properties are made. Rate equations are thus obtained for pressure, temperature and mass. Given an initial condition, the system of differential equations can be numerically integrated to obtain the cylinder conditions throughout the cycle. Once rate equations for the thermodynamic properties have been derived, it is necessary to model the various phenomena which occur during the engine cycle.

To model the combustion process, the algorithm originally proposed by Blizard and Keck (4) was extended and rederived for the Wankel geometry. The presence of two spark plugs is included in this model.

Heat transfer to the chamber walls has usually been modeled in the literature by means

*Numbers in parentheses designate References at end of paper.

0148-7191/78/0227-0416$02.50

of empirical relationships (5), or by calculating a Reynolds number for the flow related to mean piston speed via an experimentally determined codfficient and using pipe flow correlations to determine a Nusselt number (6). While these approaches may be justified in the case of a family of similar reciprocating engines once the unknown parameters have been experimentally determined, they are unlikely to apply to a Wankel in which the gas motion is determined by changes in the chamber's geometrical shape as well as by flame propagation.

To obtain a heat transfer model appropriate for the Wankel engine, McAdam's formula (7) for convective heat transfer in turbulent flow was used. . The gas velocity distribution throughout the chamber was computed by applying mass conservation equations to control volumes into which the chamber was subdivided and allowing for the flame front and regions of different chemical composition. Dimensional analysis was used to take into account inlet induced turbulence. The constant in the McAdam correlation was adjusted to match experimental data.

The model of leakage is based on the assumptions of one-dimensional isentropic flow and constant leakage area.

The quenching model couples the results of Ferguson and Keck (8), with the flame propagation model. This permitted an estimate of the gross hydrocarbon production following the method developed in a previous work (3).

Finally the real engine geometry was included through the use of analytical expressions provided by Ansdale (9) for the rotor and housi surfaces.

A Toyo Kogyo model 12 B Wankel engine was tested under both motoring and firing conditions and pressures in the chamber were measured at various locations along the engine's epitrochoidal surface. The data obtained was then used to test the ability of the model to predict the engine's performance. In order to do so four unknowns had to be determined: the effective leakage area, the coefficient in the heat transfer correlation, the entrainment speed of unburned mixture into the flame front, and the "characteristic" laminar burning time of the turbulent flame.

The effective leakage area and the coefficient in the heat transfer correlation were determined first from an analysis of the motoring conditions, using the different speed dependence of the two phenomena to uncouple them. Their determination was then repeated for the firing case. While the heat transfer correlation coefficient was the same under the both conditions, the effective leakage area was smaller during firing as has been found by Eberle and Klomp (2).

Values for the entrainment speed and characteristic burning time were determined by performing a series of parametric studies at one set of experimental conditions. Having determined all unknown values for one case, compari-

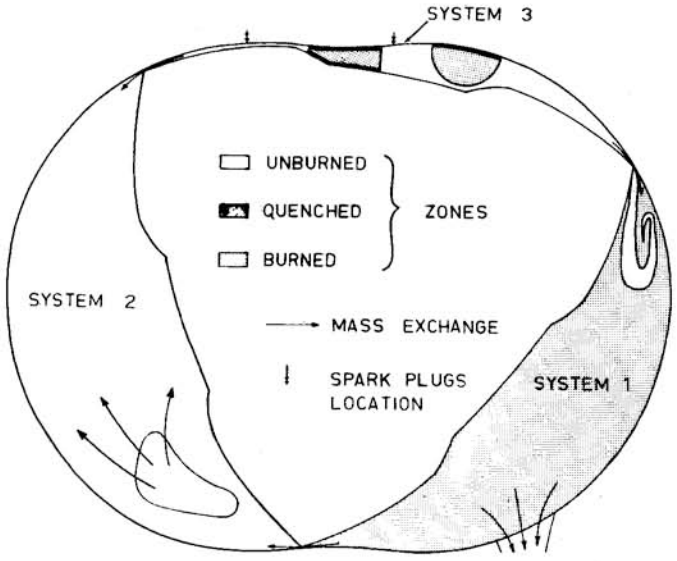

Fig. - Schematic of the engine. Each chamber is considered as an open system which interacts with other chambers and the environment. Also shown are different zones with each system

sons were then made at different conditions to see how the model fitted the other experimental data. Predictions showed reasonable agreement with the measured data.

Finally the model was used to determine possible performance gains that could be obtained from mass and heat loss reduction.

THERMODYNAMIC AND FLUID MECHANICAL MODEL

The major assumptions are:

1) Each chamber can be considered as an open system containing different gaseous zones (burned, unburned and quenched gases) subject to quasi-static processes and obeying the thermodynamic laws;

2) The pressure is uniform at each instant of time throughout each chamber;

3) The average enthalpy, energy and specific volume of each zone can be computed at each instant of time from its average temperature, pressure and composition;

4) The enthalpy associated with any mass flux between a chamber and the environment or between zones can be computed from the average thermodynamic properties of the given zone or environment;

5) The chemical composition of any gas leaving a chamber or any zone is equal to the average chemical composition for the chamber or zone.

Let us examine these assumptions. The first implies that we are dealing with thermodynamic systems whose successive states can be treated as a sequence of equilibrium states. Figure 1 shows a schematic of the engine in which the processes occurring in each chamber are intake, combustion, and exhaust. Each of the three chambers is considered as a separate system in the thermodynamic model. The model describes the processes occurring in a single chamber. Information about the thermodynamic state of the other chambers is needed only to compute leakage rates. The figure shows the different zones which are present in both the chamber where combustion is occurring (system 3) and the exhausting chamber (system 1).

The validity of uniform pressure, the second assumption, has been demonstrated for reciprocating engines. In rotary engines the flow field does indeed produce disturbances to the pressure field but Danieli (10) has shown the effect to be small.

The third assumption was tested and shown to be sufficiently accurate for engine performance calculations. At temperatures above 1000 K (11), the combustion products are assumed to be in thermodynamic equilibrium. For burned gases below 1000 K and for mixtures of fuel vapor, air and residual gas, a frozen composition is assumed with specific heats approximated by polynomial functions of temperature (12).

The fourth and fifth assumptions (similar in nature) become increasingly accurate as the number of subsystems increases. In the absence of large temperature or composition gradients within a given subsystem, they are reasonable approximations.

The basic equations for the thermodynamic model are:

1) The energy equation for each zone considered as a seperate open system

$$\dot{E} = \dot{m}_{in}\, h_{in} - \dot{m}_{out}\, h_{out} - \dot{Q} - \dot{W} \qquad (1)$$

where E, Q and W are energy, heat loss and work output, and $\dot{m}$ refers to mass flow rate entering or leaving the zone and h is the specific enthalpy associated with the mass flux;

2) The mass conservation equation

$$\dot{m} = \dot{m}_{in} - \dot{m}_{out} \quad ; \qquad (2)$$

3) The perfect gas law in differential form

$$\dot{p}\, V + p\, \dot{V} = \frac{d}{dt}\left(\sum m_i\, \overline{R}_i\, \overline{T}_i\right) \qquad (3)$$

where the sum is extended over the various zones in a chamber and

4) The definition of enthalpy

$$H = E + p\, V \qquad (4)$$

Equations 1-4 can be solved for the time rates of change of pressure and temperature of the i^{th} zone to give expressions of the form

$$\dot{p} = f_1(p,\, V,\, T_j \ldots x_j \ldots Q_j \ldots) \qquad (5)$$

$$\dot{T}_i = f_{i+1}(p,\, V,\, T_j \ldots x_j \ldots Q_j \ldots) \qquad (6)$$

where index j refers to the various zones, including the i^{th}, and x_j represents mass fractions of various component gases.

Given a set of initial conditions and the models of the various phenomena occurring during the engine cycle discussed below, the system of differential equations can be numerically integrated using the method of Krough (13) to compute the engine's thermodynamic state at each instant of time. The full derivation of this model, too long to be included here, is given in reference (10) or (14).

A. TURBULENT FLAME PROPAGATION - The turbulent flame propagation model is based on the following assumptions:

1) There is a characteristic eddy scale within the turbulent flow field below which combustion is laminar;

2) This scale is much larger than the laminar flame thickness;

3) The mechanism of combustion propagation over scales larger than the above scale is the turbulent transport of thermal energy and radicals;

4) The volume and mass of gases included within the region where the fuel oxidation reaction occurs are at any time vanishingly small compared to the mass present in the chamber.

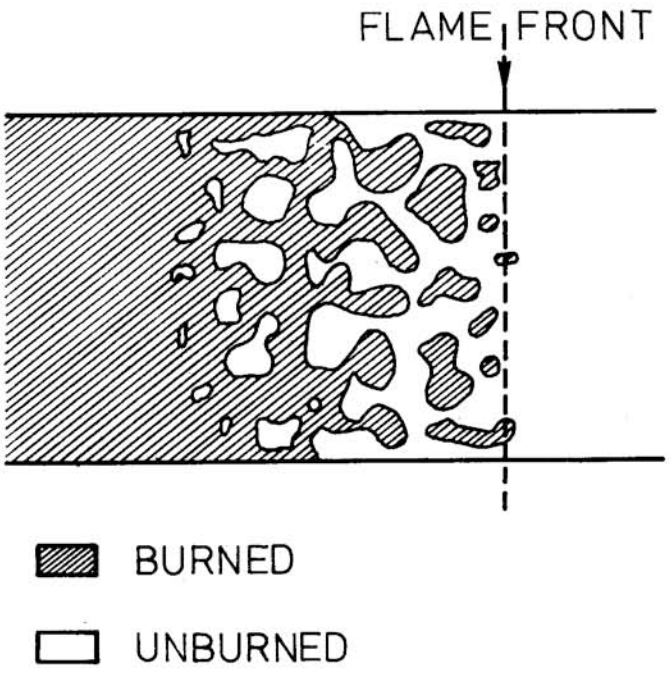

Fig. 2 - Propagation of turbulent flame in a duct

These assumptions form the basis of the Blizard and Keck model (4), and are repeated here.

Calling ℓ_e the characteristic laminar burning scale, and S_u the laminar flame speed, we can identify

$$\tau = \ell_e / S_u \tag{7}$$

as the characteristic eddy burning time.

As a consequence of the assumptions listed, we can identify three different regions in the chamber as shown in Fig. 2. One, to the left, in which only burned gases are present, another to the right in which only unburned gases are present and finally a central region in which there is an ensemble of eddies that are burning at various degrees of completion. We will define as "entrained" those gases enclosed within the outer edge of the flame front, i.e. to the left of the dashed line in Fig. 2. Since it has been assumed that within the turbulent flame unburned elements burn in the characteristic time τ, it follows that the local mass burning rate will be given by

$$\dot{m}_{b_{local}} = dm_u / \tau \tag{8}$$

If we further assume that τ is spatially constant, we can integrate over space to obtain

$$\dot{m}_b = (m_e - m_b) / \tau \tag{9}$$

where

$$m_e = \int_0^t u_e A_f \rho_u \, dt' \tag{10}$$

is the total mass entrained by the flame front at time t, u_e is an effective "entrainment speed", A_f is the flame front area, ρ_u the density of unburned mixture and time 0 refers to the ignition time. A geometrical model for the flame front area is described in the next paragraph. In the present paper the values of the characteristic burning time τ and the entrainment speed u_e were chosen to give the best fit to the data. An alternative approach involving the calculation of τ from equation (7) is given in reference (15).

B. FLAME GEOMETRY - Following Blizard and Keck (4) the flame front is assumed to propagate initially as a hemispherical shape. The hemispherical configuration of the flame front is transformed into a half sphere truncated at the height determined by the distance h between the housing and the rotor face. The truncated hemishpere is then allowed to grow until it touches the housing sides. After this occurs a one-dimensional model for circumferential flame propagation is used.

The computation is carried out as follows. Once the flame emerges from the spark plug cavity, the center of mass of the burning gases is assumed to move with the surrounding gases. From this instant on it is necessary to keep track of the original combustion center in order to compute the position and area of the flame front. This is done by determining the fraction of the mass enclosed between the trailing apex and the perpendicular to the rotor surface through the spark plug location when the flame first enters into the main chamber. In the absence of leaks, this mass fraction always defines the location of the original combustion center. With gas leakage at the apex seal, it is necessary to account for the fact that the mass left between the trailing apex and the combustion center will be continuously reduced.

Having so defined the original combustion center, entrained volumes are then computed from the expression

$$V_e = m\left[\frac{x_e - x_b - x_q}{\rho_u} + \frac{x_b}{\rho_b} + \frac{x_q}{\rho_q}\right] \tag{11}$$

where x_e, x_b, and x_q are the mass fractions of entrained, burned and quenched gases. Finally entrainment areas are computed by equating entrained volume to that computed through the geometrical model.

With two spark plugs, two combustion centers are defined and each is analyzed as outlined above. The flame fronts propagating towards each other eventually meet and entrainment at these fronts then ceases.

C. HEAT TRANSFER MODEL - The heat transfer model is based on a correlation between Nusselt number and Reynolds number of the form

$$Nu = c_1 \, Re^{0.8} \tag{12}$$

When applied to reciprocating piston engines where the gas speed is unknown, the Reynolds numbers are usually computed on the basis of piston speed and the constant c_1 is then emperically determined (as in the work of Woschni (6)). This traditional approach has not been followed in the present work; an approach similar to the one followed by Bracco and Sirignano (1) has been used instead. The average gas speed at a given cross section is determined by applying mass conservation to the volume enclosed by the trailing apex seal and the section considered. This gives

$$\frac{dm}{dt} = \rho\ u\ A + \dot{m}_{\ell t} \tag{13}$$

where ℓ refers to leakage and t to the trailing apex. Observing that the mass rate of change can be written as a function of densities and partial volumes of the enclosed gases and their time rates of change (which can be computed from the thermodynamic and geometrical models), the average speed at the given section is thus determined. Notice that this is basically an inviscid solution for the flow field and that the boundary layers must be thin for a uniform velocity profile to be a valid approximation.

The gas motion induced within the chamber by the intake and exhaust processes is also computed. This is done by assuming a point mass sink or source of appropriate strength at the port location while the intake or exhaust processes are occurring. (The method used to compute the mass flows through the intake and exhaust is described in Section E below.)

The flux of kinetic energy into the chamber E_{KE} is given by

$$\dot{E}_{KE} = \tfrac{1}{2}\ \dot{m}\ \bar{u}^2 \tag{14}$$

where $\bar{u}$ is the mean speed of the incoming flow. (The kinetic energy of the turbulent fluctuations in the intake flow has been neglected) This jet flow will be transformed into turbulent flow, the specific turbulent kinetic energy e is dissapated at a rate ε given by

$$\varepsilon = (2e/3)^{3/2} \ / \ \ell \tag{15}$$

where ℓ is a characteristic dissipation length. Thus the average turbulent kinetic energy E_T of the gas motion within the chamber at any time t after the inlet valve opens is given by the time integral of the difference between the energy flux into the chamber and the dissipation rate, i.e.

$$E_T = me = \int_0^t \left[\tfrac{1}{2}\ \dot{m}\ \bar{u}^2 - \frac{m(2/3\ e)^{3/2}}{\ell} \right] dt' \tag{16}$$

ℓ is known a priori, but we know from the experiments of Windsor and Patterson (16) the decay time of turbulence in a reciprocating engine. We can therefore fit the value of ℓ to obtain the proper decay. Once this is determined during intake and compression the turbulent fluctuating velocity

$$u' = (2/3\ e)^{1/2} \tag{17}$$

can be computed. This fluctuating velocity component is added orthogonally to the computed gas speed due to the changing shape of the chamber, and intake mass flow, to obtain a local velocity vector. Once this velocity field is known, heat transfer is computed on the rotor and housing surfaces separately with Eq. (12). The local hydraulic diameter is used for the length scale; account is taken of the different gas speeds relative to the rotor and housing, and for different wall temperatures. The wall temperatures are assumed to be constant and their values are based on measurements by Yamamoto (17).

D. QUENCHING MECHANISM - Ferguson and Keck (8) propose for quenching distance the use of the relation

$$\delta_q = c_2\ P_e\ \alpha_u\ /\ S_u \tag{18}$$

where c_2 is a constant, α_u the thermal diffusivity, S_u the laminar flame speed, and P_e the Peclet number. The Peclet number at quenching is a relatively weak function of the thermodynamic variables and is computed at the location at which the rate of energy release due to combustion exactly balances the rate of energy loss due to heat transfer. This relation was preferred to others (e.g. (18)) because it contains in α_u and S_u a dependence on pressure, temperature, air fuel ratio and exhaust gas recirculation fraction.

A quenching thickness is computed through this algorithm and, since the areas covered by the burned gases are known, the mass quenched can be computed at each instant of time from the expression

$$\dot{m}_q = \rho_u\ \delta_q\ \dot{A}_b \sim \rho_u\ \delta_q\ A_b\ \dot{V}_b\ /\ V_b \tag{19}$$

where A_b is the surface "wetted" by the burned gases. Note that the last expression is an approximation valid for the Wankel engine given its "stretched" configuration.

E. LEAKAGE AND GAS EXCHANGE MECHANISMS.- Assuming that the flow through the leakage area is a quasi-steady one-dimensional isentropic flow, and that the intake and exhaust systems are large plenums, the mass flow rate between chambers or between chamber and intake or exhaust plenums may be computed according to the equations given by Shapiro (19):

$$\frac{\dot{m}_{jk}}{m_j} = \frac{C_d\ A_{jk}}{V_j}\ \gamma_j\ R_j\ T_j \left(\frac{2}{\gamma_j - 1} \left[\left(\frac{P_k}{P_j}\right)^{2/\gamma_j} - \left(\frac{P_k}{P_j}\right)^{(\gamma_j+1)/\gamma_j} \right] \right)^{1/2} \tag{20}$$

for

$$\frac{P_u}{P_k} < \left[\frac{\gamma_j + 1}{2}\right]^{\gamma_j/(\gamma_j-1)} \tag{21}$$

and

$$\frac{\dot{m}_{jk}}{m_j} = \frac{C_d A_{jk}}{V_j} \gamma_j R_j T_j \left(\frac{2}{\gamma_j + 1}\right)^{(\gamma_j+1)/2(\gamma_j-1)} \tag{22}$$

for

$$\frac{P_j}{P_k} \geq \left(\frac{\gamma_j + 1}{2}\right)^{\gamma_j/(\gamma_j-1)} \tag{23}$$

where indexs j and k denote upstream and downstream conditions, respectively, and C_d is the discharge coefficient of the discharge area A_{jk}.

Flow coefficients used in the calculations were 1.0 for all leakage areas since these areas are not well defined. For the exhaust port the coefficients of 0.75 and 1.0 were used for outflow and inflow, respectively, while for the intake port the values used were 0.5 in outflow and 1.0 in inflow. These choices were made to try to reproduce as closely as possible the observed pressures during the gas intake and exhaust precesses.

One last observation concerns the period of port overlap. Since intake and exhaust ports are both open for a period, it is likely that some residual gas is sucked into the intake manifold. The outflow of residual gases into the intake was integrated during port overlap and the burned mass was reintroduced into the engine during the intake process.

F. GEOMETRICAL MODEL - In the geometrical model it is assumed that the housing profile is an epitrocoidal curve of radius r and eccentricity e, displaced by a constant distance a from the pure epitrocoid, and that the rotor profile is a pure ipotrochoid on which a linearized cavity is added. All geometrical computations are carried out through numerical integration, in order to allow any value of a and any cavity shape to be specified. A complete description of the geometrical model, based on the equations provided by Ansdale (9), is given in reference (14).

EXPERIMENTAL APPARATUS AND BASIC MEASUREMENTS

Figure 3 is a schematic representation of the experimental apparatus. The test engine was a Toyo Kogyo series 12 B twin rotary Wankel engine. Table 1 contains its main geometrical parameters. Water and oil cooling systems were modified by providing external electrically driven pumps and heat exchangers able to exchange heat in both directions. This was done to allow engine warm-up before starting to reduce wear, and to allow the motoring of the engine in a "hot walls" condition.

Since one of the aims of this study was to measure performance changes as the air-fuel ratio was varied independently of load and speed, the carburator of the production engine was removed and replaced by a steam jacketed mixing tank. Fuel was introduced into the tank via an atomizer. The fuel atomizers used (Delevan) provided a fuel flow that was a known function of the atomizing pressure. This provided a reliable way of measuring fuel flow. Three fuel atomizers were used to cover the entire speed and load range of the engine, so the atomizers always operated in the pressure range that would assure a small enough maximum droplet size.

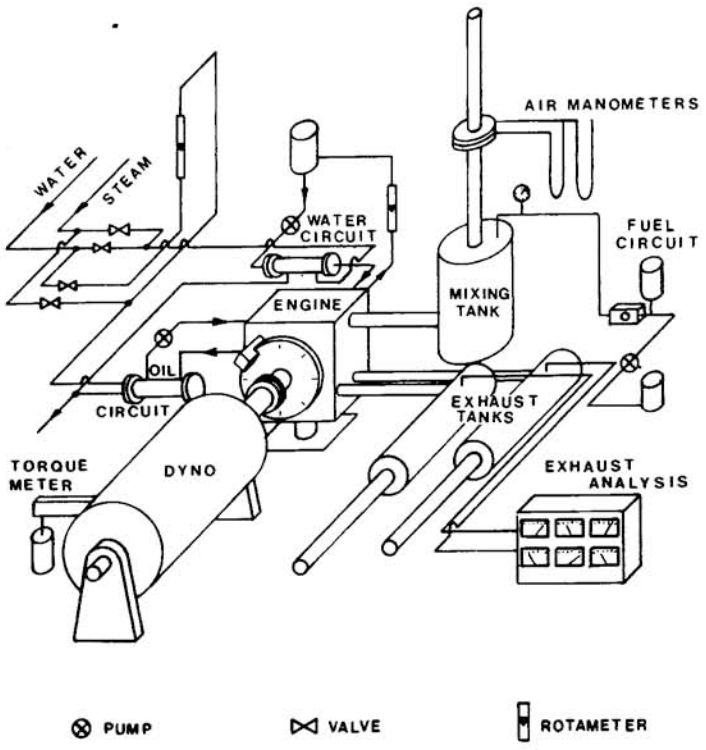

Fig. 3 - Experimental apparatus

Table 1 - Engine Parameters

Manufacture: Toyo Kogyo Co. Ltd.		
Model: 12 B		
Twin rotary engine, water cooled		
Displacement:		573 cm^3 x 2 rotors
Compression ratio:		9.4
Crankshaft eccentricity:		15 mm
Housing generating radius:		102 mm*
Housing displacement from true epitrochoidal:		3 mm*
Rotor generating radius:		104.5 mm**
Port timing:		
Intake opens	-508	BTDC
Intake closes	-220	BTDC
Exhaust opens	199	ATDC
Exhaust closes	-491 30'	BTDC

* Courtest of Toyo Kogyo Co., Ltd.
** estimated

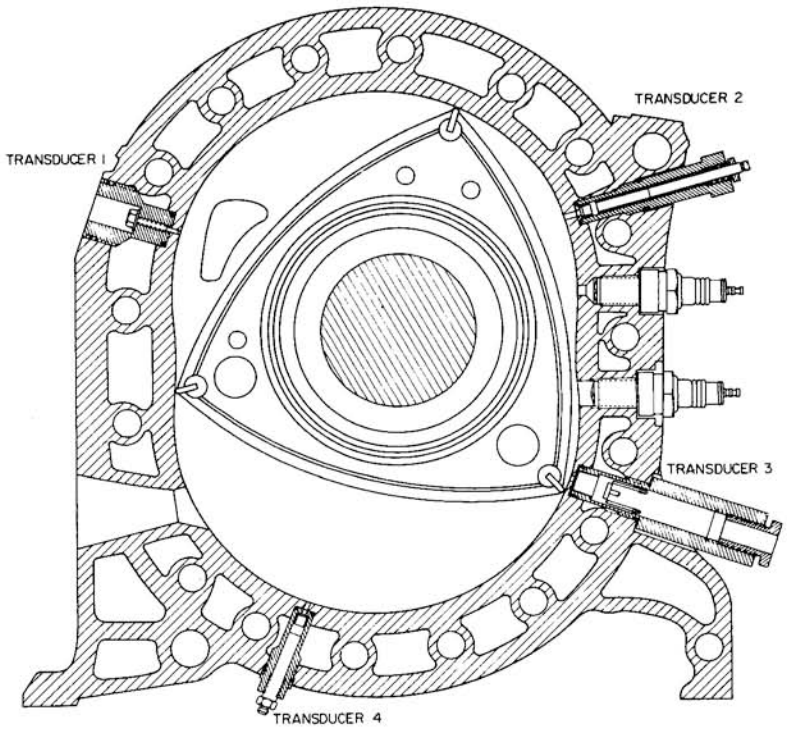

Fig. 4 - Cross-section of the engine showing the pressure transducer locations

Air flows were measured with two ASME square edged orfices (one for high and one for low speed) in order to minimize errors on the low-speed end of the scale.

Ignition was provided by using the standard ingition system of the engine, but timing was adjusted at each condition to obtain maximum brake torque. Torque was measured with a standard M.I.T. hydraulic scale. Water, oil and intake flow temperatures were measured with iron-constantane thermocouples, individually calibrated before introduction in the engine setup. Exhaust gas temperatures were measured with a chromel alumel thermocouple manufactured by Omega Co.

For mixing and exhaust tanks and intake orifice static pressures were measured with manometers (water or mercury).

The estimated error for the above measurements was $\pm 2\%$. Ignition timing was adjusted to ± 0.5 CA°.

Five different pressure transducers were used to record the pressure inside the combustion chambers. Four of these were mounted on the rear chamber as shown in Figure 4, and one was mounted on the front chamber in a spark plug adapter. The first four transducers installed in one chamber provided a continuous pressure record of the full engine cycle while a fifth was installed to check the performance of the second chamber by monitoring the pressure during the combustion phase. This was the best position to detect any differences in the performance of the two chambers. The transducers used were (referring to Figure 4):

Transducer 1	Kulite	Model XTMS-1-190-50
Transducer 2	PCB	Model 111A24
Transducer 3	AVL	Model 8QP 500 ca
Transducer 4	Kestler	Model 601A

The fifth transducer, installed in the front chamber, was a PCB Model 111 A 24 with a spark plug adapter No. 65 of PCB catalog. The wide variety of transducers used was the result of spatial constraints (presence of studs that made necessary the use of narrow transducers) and experimental requirements. A strain gauge transducer was used on the intake side to measure absolute pressure.

Because of geometrical constraints, only one of the transducers was provided with an independent water cooling system. The others were operated at the water jacket temperature. Hence the calibration of these transducers, obtained at room temperature with a dead-weight tester, had to be corrected for the temperature change. This correction was made by taking as a standard the output of the water cooled transducer and performing a best fit of the data from the other transducers. The method is described in detail in reference (14). The observed deviation from dead weight tester calibration was small (less than 5% in the worse case). To avoid "thermal cycling" of the transducers (20) a coating of RTV was applied to reduce the effects of the gas temperature variation on the transducer surface.

Angle measurements were made with a digital clock, coupled to a counter and a trigger reset. The system was calibrated statically by making

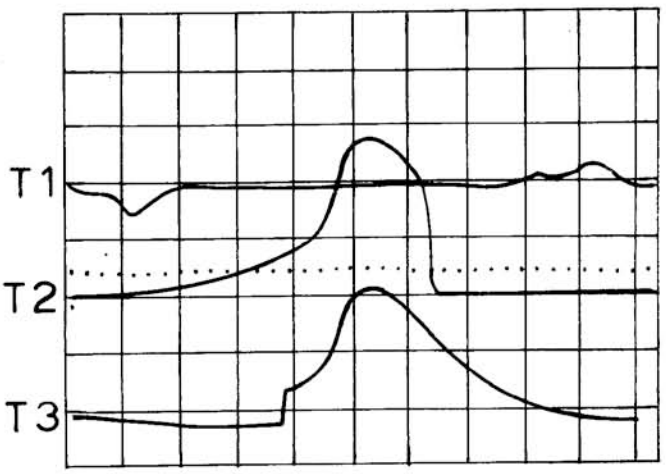

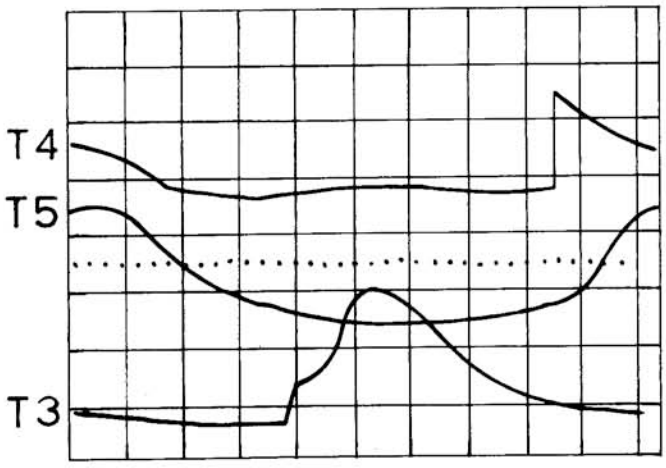

Fig. 5 - Oscilloscope records showing outputs of various transducers and of crank angle indicator (dots)

sure that the reset signal corresponded to a known engine position (TDC mark on the front pulley for the front rotor) and dynamically by triggering a strobe light, shining on the front pulley, from the reset signal with the engine rotating at different speeds. The estimated error was less than ±0.5 crank angle °.

Two separate exhaust tanks were provided for independent exhaust gas analysis on both rotors. The exhaust gas analysis was carried out with the following instruments:

1) Scott Paramagnetic Oxygen Analyzer Model 150
2) Beckman Infrared CO Analyzer Model 864
3) Beckman Infrared CO_2 Analyzer Model 315A
4) TECO Chemilumenscent NO Analyzer Model 10A
5) Scott Heated Hydrocarbon Analyzer Model 215

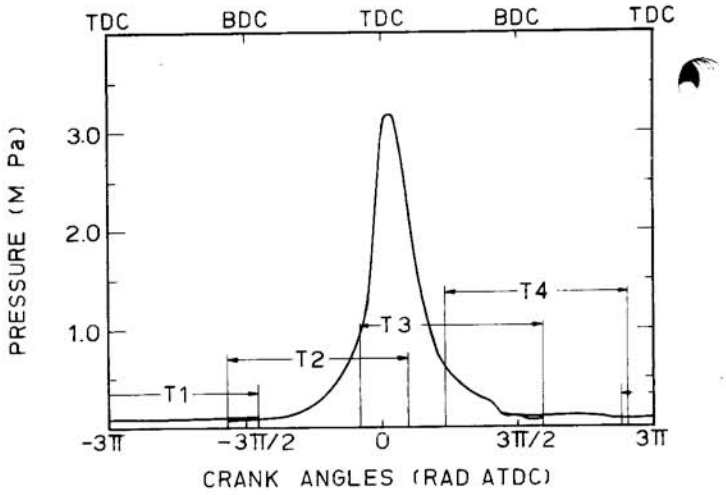

Fig. 6 - Complete pressure diagram obtained from previous record, and regions of transducer recording

Finally the engine was fueled with a mixture of isooctane and 2 per cent of Texaco Ursa oil L.A.3 to compensate for the removal of the oil metering pump when the mixing tank was added.

A. PRESSURE MEASUREMENTS - Figure 5 shows a typical set of pressure oscillograms for the four transducers on the front chamber while Figure 6 shows the same data pieced together along with the angular ranges covered by each transducer.

Since both the pressure and torque were measured under firing and motoring conditions the following equation was examined:

$$\int_0^{6\pi} P_{fir} dV/V_d = BMEP_{fir} - BMEP_{mot} + \int_0^{6\pi} P_{mot} dV/V_d \quad (24)$$

where the subscripts fir and mot refer to firing and motoring conditions and V_d is the displacement volume. This is an exact equality only if the friction during motoring and firing conditions are identical. This may be an acceptable approximation since, although during firing the load on the crankshaft is higher, the oil viscosity drops due to the higher temperature. Table 2 shows the results of this computation. An average error of -0.06% was recorded, while the standard deviation was 3.5%. The agreement is again judged excellent.

B. EXHAUST ANALYSIS COMPARED TO AIR AND FUEL FLOW MEASUREMENTS. - Exhaust concentrations of CO, CO_2, O_2, HC and NO were measured. The method of Spindt (21) was used to compute the fuel-air ratio equivalence ratio of the original mixture. This is also given by individual flow measurements of air and fuel. Fuel-air equivalence ratios, as computed from the exhaust gas analysis applied to each rotor's exhaust separately, were in agreement, while an average

Table 2 - Analysis of Experimental Pressure Data
(Pressures in K P_a)

Run	RPM	$BMEP_{fir}$	$BMEP_{mot}$	$\int_o^{6\pi} P_{mot} dV/V_d$	$\int_o^{6\pi} P_{fir} dV/V_d$	IMEP*	$\frac{\int P_{fir} dV - IMEP \times V_d}{IMEP \times V_d}$ %
8	2040	468	-129	-94	474 - 484	503	-4.8
9	2070	324	-121	-93	355 - 348	352	-0.1
10	2040	176	-133	-108	205 - 217	201	5.5
11	2070	324	-129	-102	359	351	2.3
12	2080	211	-131	-93	264 - 221	249	-2.2
13	1020	215	-133	-92	247 - 282	256	2.1
14	3960	363	-203	-136	429 - 410	430	-2.4

* $IMEP = BMEP_{fir} - BMEP_{mot} + \int_o^{6\pi} P_{mot} dV/V_d$

Average error IMEP 0.06%
Standard Deviation 3.5%

Table 3 - Fuel Air Equivalence Ratios Analysis as Computed from Flow Measurements and from Exhaust Composition

Run	Load	RPM	Φ_{flow}	Φ_{front}	Φ_{rear}	$(\Phi_{ave} - \Phi_{flow})/\Phi_{flow}$ %
8	Max	2040	1.04	1.00	1.00	-3.8
9	Mid	2070	1.02	1.02	1.02	0.0
10	Low	2040	.99	.99	1.00	0.5
11	Mid	2070	1.26	1.23	1.23	-2.4
12	Mid	2080	.85	.81	.80	-5.1
13	Mid	1020	1.05	1.06	1.05	0.5
14	Mid	3960	1.08	1.05	1.04	-3.2

Average error on Φ -1.45%
Standard deviation 2.5 %

error of -1.6% was registered between flow measurements and exhaust gas analysis (the equivalence ratio based on measured air flow being richer). The results of this analysis are presented in Table 3.

C. GLOBAL ENERGY BALANCE. - By writing the energy equation for an open system in steady state, one obtains the following relation

$$\left[h_u(T_{int}) - h_b(T_{int})\right] m = \left[h_b(T_{exh}) - h_b(T_{int})\right] (m - m_{HC}) + \left[h_u(T_{exh}) - h_b(T_{int})\right] m_{HC} + Q_{loss} + W_{usef} \quad (25)$$

where m is the mass flowing into the engine per revolution, h_u and h_b are the enthalpies of the unburned and burned gases evaluated at the intake (T_{int}) or exhaust (T_{exh}) temperatures, m_{HC} is the mass which leaves the engine still unburned, Q_{loss} is the heat loss and W_{usef} is the useful work. The first term represents the total energy available, the second is the energy wasted as exhaust loss due to the exhaust temperature being higher than the temperature at intake, and the third term is the energy loss due to incomplete combustion of the charge.

Several possible sources of error exist in this energy balance, such as heat lost through convection and radiation. These errors, analyzed in detail in reference (10), are not sufficient to balance equation (25), and their estimated global value is given in Table 4 for all runs as Q_{conv}, together with the other parameters of the energy balance. It is, however, important to recognize that equation (25) assumes that all of the gas that is introduced into the engine comes out in the exhaust, and has the composition measured by the exhaust gas analysis. This is not necessarily true for a Wankel engine since side seal leakage to the crankcase can be significant. Assuming the gas leaking into the crankcase is predominantly unburned, one can determine the mass m_{sl} lost in this manner by finding the value of m_{HC} required to balance equation (25) and subtracting this from the mass of hydrocarbons measured in the exhaust. Values of the calculated ratio m_{sl}/m are given in Table 4 and average about 10%. One might anticipate that the fractional mass loss should be inversely proportional to engine speed but the scatter in the data is too large to test this prediction. The presence of side seal leakage

Table 4 - Energy Balance for Various Runs and their Thermodynamic Efficiency

Run	H_{tot}	H_{exh}	H_{unb}	Q_{loss}	W_{usef}	Q_{conv}	E_{error}	$(m_{s\ell})/m$	η_{TH}
	Joules/Cycle						%	%	%
8	1221	278	83	425	268	25	12	15.4	21.0
9	833	200	70	260	186	25	11	15.0	21.7
10	599	131	56	239	101	25	8	10.3	16.7
11	798	220	66	288	286	25	2	2.3	17.4
12	719	200	71	257	121	25	6	9.1	16.7
13	714	98	103	244	123	32	16	19.0	16.2
14	893	266	47	312	208	22	4	6.2	21.1
								av.	10.6

$$E_{error} = 100(H_{tot} - H_{exh} - H_{unb} - Q_{loss} - W_{usef} - Q_{conv}) / H_{tot}$$

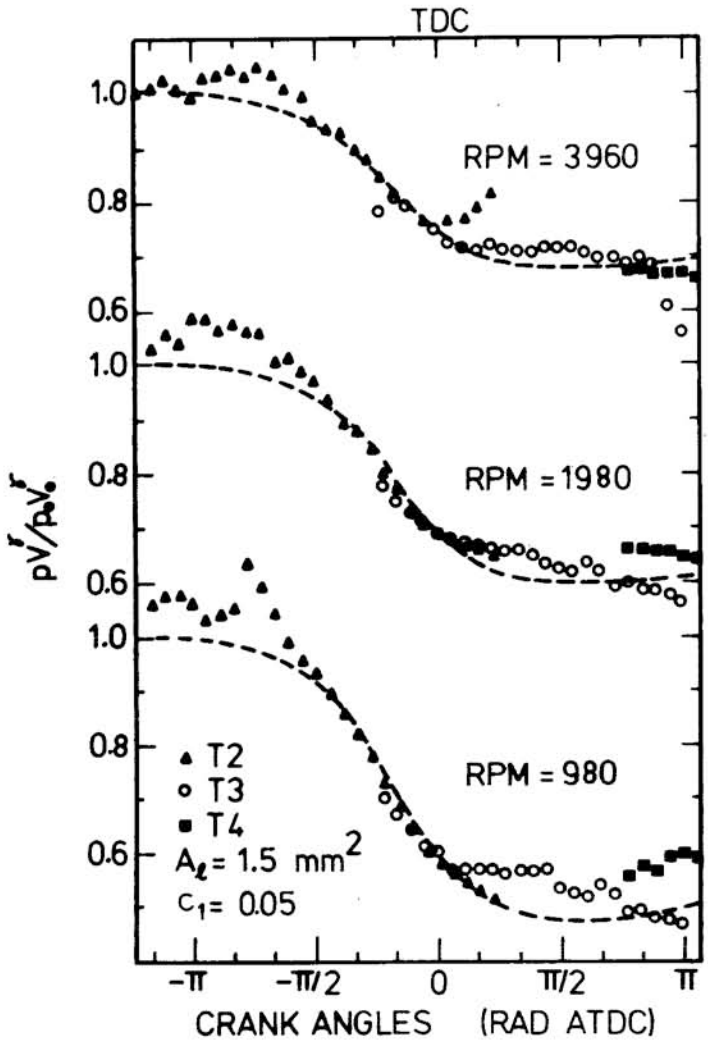

Fig. 8 - pV^γ versus crank angle obtained from the various transducers during motoring conditions, versus model predictions (dash)

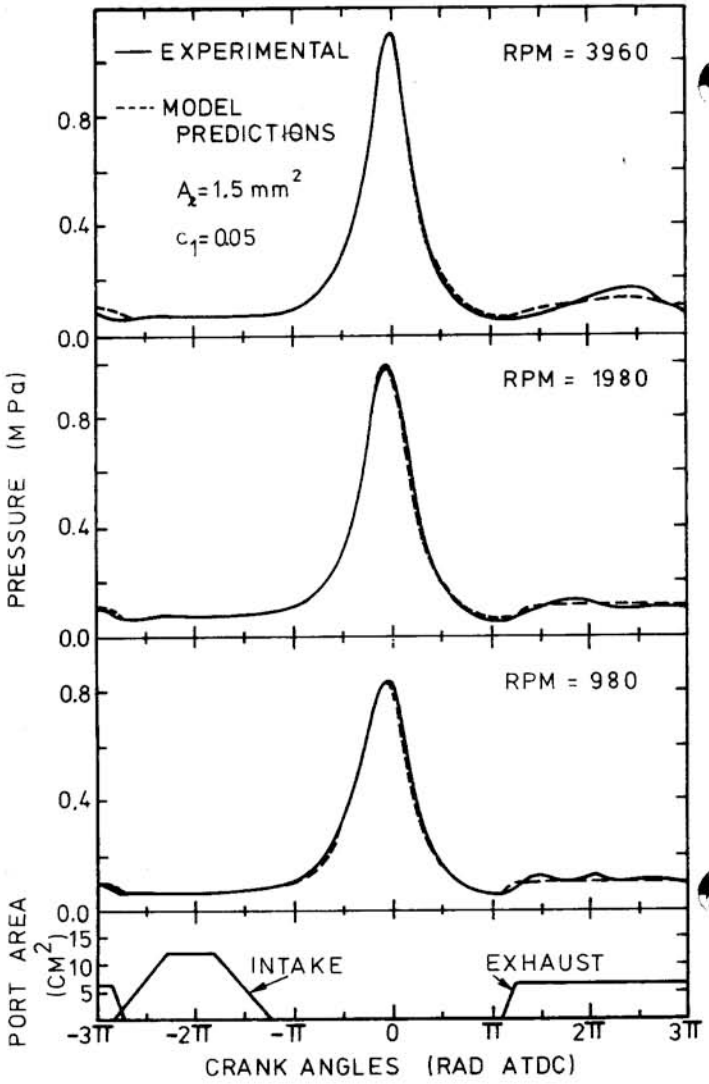

Fig. 7 - Experimental pressure diagrams obtained for the motoring cases versus model predictions

is also indicated by the discrepancy between predicted and measured mass flow rates. This will be treated in more detail in a following section.

COMPARISON BETWEEN THEORY AND EXPERIMENTS UNDER MOTORING CONDITIONS

Three parameters must be determined to calculate the performance of a motored engine. These are the characteristic decay length ℓ of the turbulence induced by the intake process (equation (15)), the constant c_1 in the Nusselt number dependence on the Reynolds number (equation (12)) and the effective seal leakage A_ℓ (assumed to be located at each apex). The value of ℓ was determined by using equation 12 to fit the data of Windsor and Patterson (16). Values for c_1 and A were obtained by fitting the data from the present experiments.

Figure 7 shows the comparison between the measured (continuous line) and calculated (dashed line) pressures as a function of crank angle for a motored engine pumping air at three

speeds. Figure 8 presents the same data as plots of $pV^{\gamma}/ p_o V_o^{\gamma}$ versus crank angles, where γ is the ratio of specific heats (1.4 for air at inlet temperatures) and the index o refers to conditions at the beginning of the compression. In this Figure the experimental data are plotted as points while the theory is, as before, the dashed line. The leakage area used in this model was A_ℓ = 1.5 mm^2 and the heat transfer correlation constant was c_1=0.05 (about 1.5 times the value used by Woschni). The reasons for these choices are discussed below.

As can be seen the agreement is generally good in the neighborhood of TDC when the pressures are high, but deteriorates somewhat at low pressures where accurate measurements are more difficult to make. One advantage of plotting the data in pV^{γ} form is the fact that it magnifies the discrepancies between predictions amd measurements at low pressures.

As can be observed, the pV^{γ} plots are not symmetric about TDC. This is due to two factors. First, the turbulence induced during the intake process (and hence heat transfer produced by the turbulent motion) decays during the compression. Second, as shown in Figure 9, the velocity produced by the changing geometrical shape of the chamber is particularly high at three crank angles -50°, TDC, and +40°. The first velocity peak is the largest and will result in the highest heat transfer rate. Figure 10 shows the calculated distribution of heat transfer as a function of time and position along the rotor surface. Notice the relative magnitude of the peak heat transfer at -50°, and at +40° on the other side of TDC.

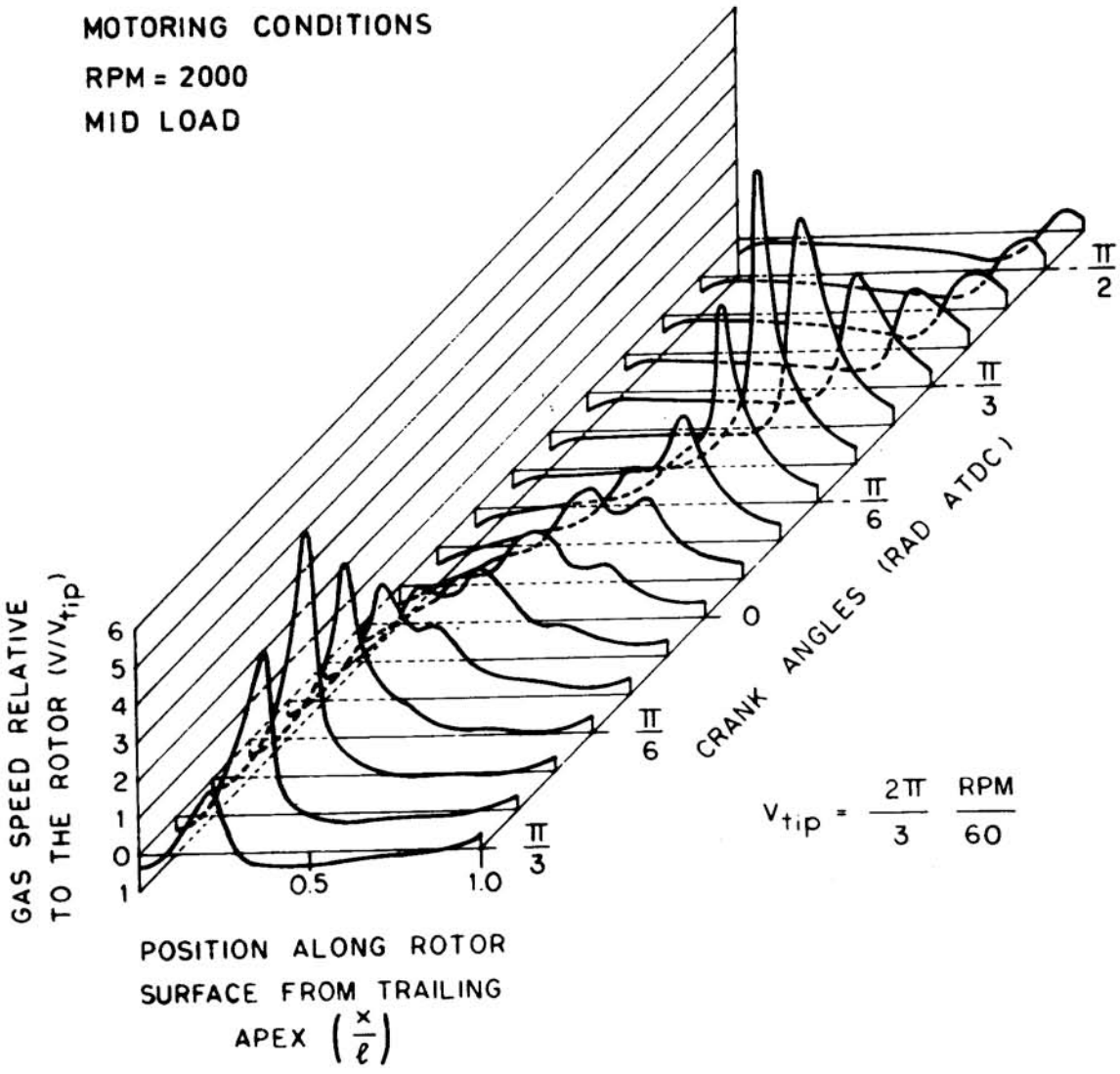

Fig. 9 - Gas motion induced by the changing chamber geometry, relative to the rotor. Positive in the direction of rotation. Nondimensionalized by the average rotor tip velocity

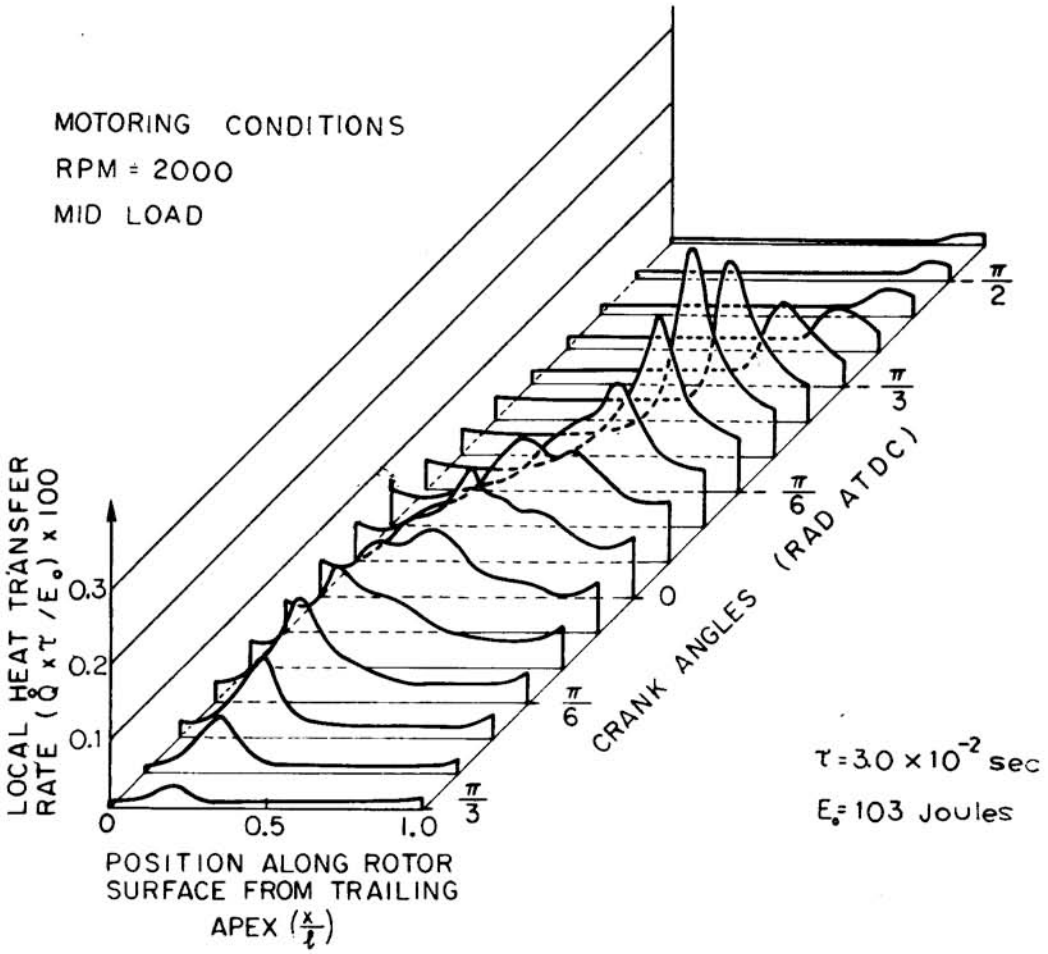

Fig. 10 - Heat transfer due to changing engine geometry versus crank angle and position along the rotor surface, divided by the energy of the system at intake port closed (E_O), and the period of one rotor revolution

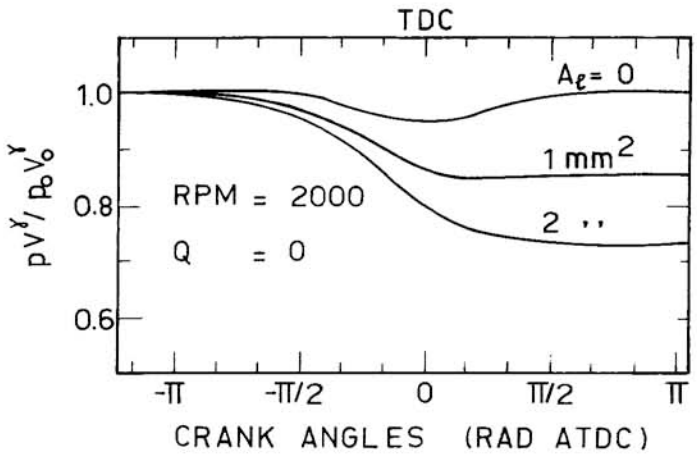

Fig. 11A - Change in pV^γ with effective leakage area per apex seal (A_ℓ) at constant speed and zero heat transfer

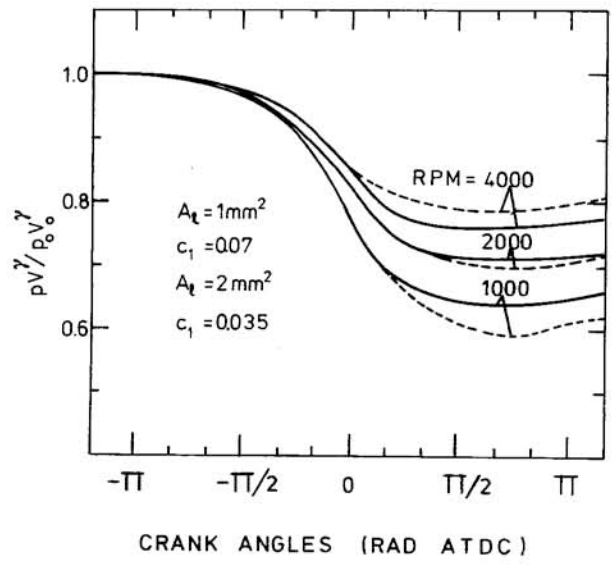

Fig. 11B - pV^γ plots showing different speed dependence for leakage and heat transfer

The best fit values of the two unknowns, A_ℓ and c_1, were determined from a parametric study where each was varied in turn. Figure 11a shows $pV^\gamma/p_oV_o^\gamma$ for three cases with varying leakage area: A_f = 0, 1, and 2 mm^2 per apex seal at constant speed with no heat loss, i.e. $c_1 = 0$. In all cases presented here, $(V/V_o)^\gamma$ was computed using a constant value of $\gamma = 1.4$. As a consequence the curve generated for the isentropic case $A_\ell = 0$ shows a minimum in the regions of TDC, where temperatures are higher and the real gas value of γ is slightly lower. Notice that this fact further destroys the anti-symmetry of the curves about TDC when there is leakage and heat transfer.

The effect of engine speed on the relative importance of heat and mass loss calculated for a Wankel engine is shown in Figure 11b. It can be seen from the relative positions of the continuous and dashed curves that at low speed mass loss dominates while at high speed heat loss dominates.

Comparison of the curves in Figure 11 with the experimental data led to the choice of $c_1 = 0.05$ and $A_\ell = 1.5$ mm^2 per seal used in Figures 7 and 8. Under firing conditions the value of c_1 is expected to be unchanged but the effective leakage area A_f may be reduced due to thermal effects discussed below. Note that for reciprocating piston engines Woschni (6) determined the heat transfer correlation constant to be $c_1 = 0.035$.

COMPARISON BETWEEN THEORY AND EXPERIMENTS UNDER FIRING CONDITIONS

A. LEAKAGE AND HEAT TRANSFER. - The parameters required to predict the performance of a firing engine are: the constant c_1 in the Nusselt-Reynolds number correlation for heat transfer, the effective leakage area per apex seal A_ℓ, the entrainment speed u_e and the characteristic burning time τ of an eddy. As mentioned in the previous section, a value for the heat transfer constant $c_1 = 0.05$ was determined from the motoring runs. A value for the effective leakage area $A_\ell = 1.5$ mm^2 per apex seal under motoring conditions was also determined in a similar way. However, it is to be expected that engine clearances will vary between motoring and firing conditions. When firing, all components of the rotor will be hotter and will expand, but the housing will be constrained in width by the studs which hold the engine together and are at the water jacket temperature (approximately the same in both cases). The use of the leakage area found for motoring led to pressures during firing which were too low, implying that the leakage area was too large. A leakage area of $A_f = 1$ mm^2 per apex seal during firing gave the best fit. This different behavior between motoring and firing conditions has also been found and reported by Eberle and Klomp (2) who also measured a leakage area of 1 mm^2 for a different engine.

To determine the values of the entrainment speed u_e and characteristic burning time τ it was decided to use the base condition 2000 RPM, mid-throttle setting and stochiometric fuel-air ratio, (Run #9). A parametric study was then made to find the best fit by first varying the entrainment speed between u_e = 4 and 8 m/s with a characteristic burning time τ = 0.5 ms. (corresponding to a combustion delay of about 6 degrees of crank angle at this speed). The results are presented in Figure 12 which shows plots of both $pV^\gamma/p_oV_o^\gamma$ and pressure as a function of crank angle. In this figure the index o refers to ignition conditions. The values of γ used are different for the combustion and the combustion-expansion phases, and are the ones given by Danieli et al (3) obtained by fitting data for real gases using constant local specific heats. Next the entrainment speed was held constant while τ was varied from 0.2 ms to 0.8 ms.

On the basis of these parametric studies the "best values" of τ = 0.5 ms and u_e = 6 m/s were determined. This was done by matching the initial rise in pressure and pV^γ rather than final level of pV^γ because for determining τ and u_e the burning phase was felt to be the most important part of the cycle.

The value of the constant in the Nusselt number dependence on Reynolds number that gave the best fit to the pressure data was then determined to be approximately $c_1 = 0.05$ the same

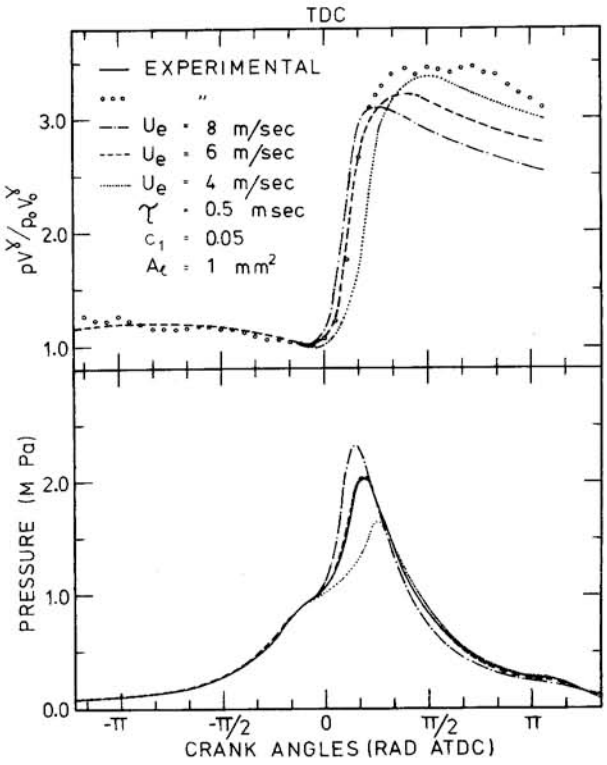

Fig. 12 - Effects of entrainment speed on pV^γ and pressure, during firing conditions, holding other parameters constant

Table 5 - Comparison of Measured and Predicted Values of Mass Intake Per Cycle, IMEP, Heat Loss Per Cycle and Work Output Plus Heat Loss Per Cycle

Run	Mass			IMEP			Heat			W + H		
	exp.	th.	err.	exp.	th.	err.	exp.	th.	err.	exp.	th.	err.
	Kg. x 10^4		%	k Pa		%	J/cycle		%	J/cycle		%
8	4.69	4.17	-9	503	554	10	433	387	-10	721	704	-2
9	3.04	2.72	-10	352	349	-1	268	283	6	470	483	3
10	2.20	1.87	-15	200	198	-1	247	216	-13	362	329	-9
11	3.11	2.64	-15	351	301	-14	296	257	-13	497	430	-14
12	3.05	2.30	-25	248	238	-4	266	225	-15	408	361	-11
13	2.63	2.41	-12	259	195	-25	252	247	-2	400	359	-10
14	3.32	3.10	-6	430	430	0	295	251	-15	541	497	-9
Average error			-13			-5			-9			-8

value obtained from the analysis of the motoring runs. This was done by matching predictions against the entire data base.

Using the values of the parameters determined by fitting the pressure vs crank angle data in the manner described above, calculations were then made of the mass intake per cycle, the mean effective pressure, the heat loss per cycle and the combined heat loss and work output per cycle for all the conditions investigated. The predictions are compared with measured values in Table 5. It can be seen that our model still underpredicts mass intake as well as work and heat outputs. Morever, the error in the mass is, on the average, bigger than the error made in heat and work combined. Such an error cannot be caused by the use of one dimensional isentropic flow relations to compute gas intake. This could cause only minor departures from the value of the mass actually inducted, since the dynamic effects were greatly reduced during intake by the experimental set up.

On the other hand, a parametric study of the effect of the leakage area showed that it strongly effects mass intake, residual fraction and IMEP. This is shown in Figure 13. To match the measured mass intake, the leakage area would have to be so small that it would result in unacceptably high power outputs. This is also shown by Figure 14 which displays the effect of the leakage area on pressure vs. crank angle history. On the same figure we can also see that there is a mismatch between predicted and measured values of pV^{γ}. If leakage areas were reduced, the comparison between theory and experiments on pV^{γ} would look better, but the power output match would be worse. The mismatch on the overall energy balance, discussed in a previous section, was attributed to side seal leakage. The model does not take into account leakage past the side seals, but assumes all leakage occurs past the apex seals. The error introduced by assuming that all leakage goes into the other chambers is not important when one tries to match theoretical predictions with experiments in the region of high pressures. This is because it is immaterial where the gas goes, as long as it leaves the system. On the other hand, if the side seal leakage is important some of the mass that leaves the high pressure

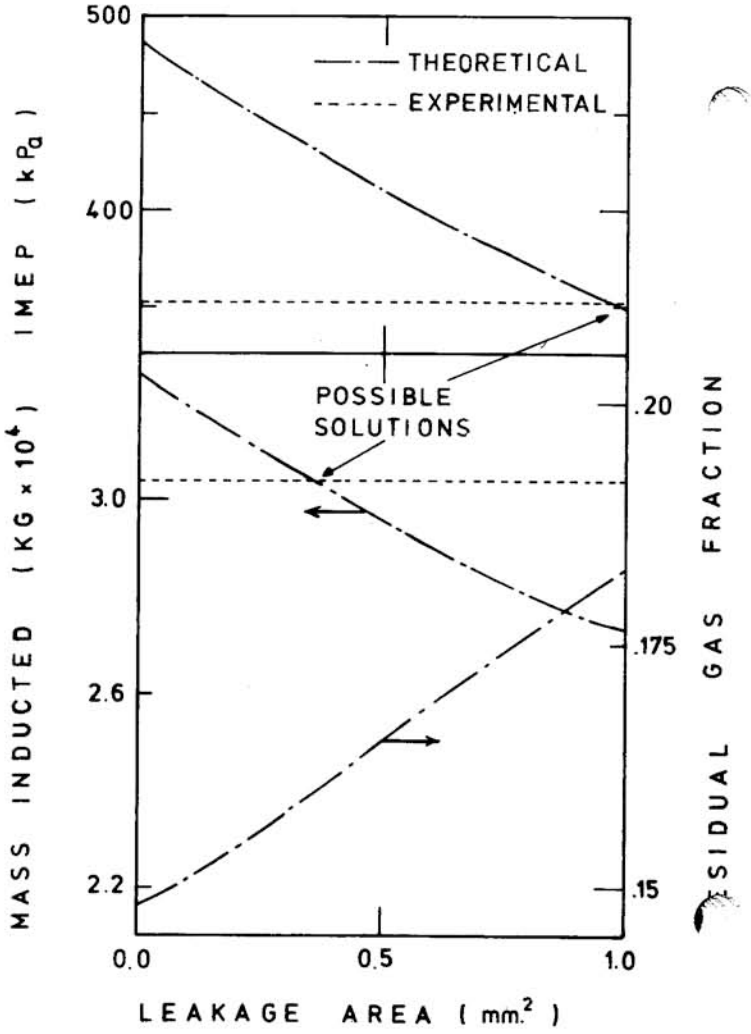

Fig. 13 - Effect of leakage area on mass and residual fraction, holding other parameters constant

chamber will be lost through the oil pan to the atmosphere. Hence overall, less mass will leak into the inducting chamber and as a consequence more mass of fresh mixture will enter the system. Note that the average value of the error in the mass due to side seal leakage, as estimated from the mismatch on the energy balance ($m_{s\ell}/m$ of Table 4), is of the same order as the observed error between theoretical and measured mass inflows. It is quite clear that more work is needed to investigate the influence of side seal leakage. Eberle and Klomp (2) also investigated the effects of side seal leakage but their conclusions do not necessarily apply to our engine due to differences in seal design.

As noted before there is a mismatch between measured and predicted values of the jump in pV^{γ}. We discarded as a possible reason the influence of the leakage area. A parametric study of the effect of the heat transfer correlation coefficient on pV^{γ} was then made. Results of this study, reported in detail in reference (15), showed the jump to be essentially unaffected by heat transfer.

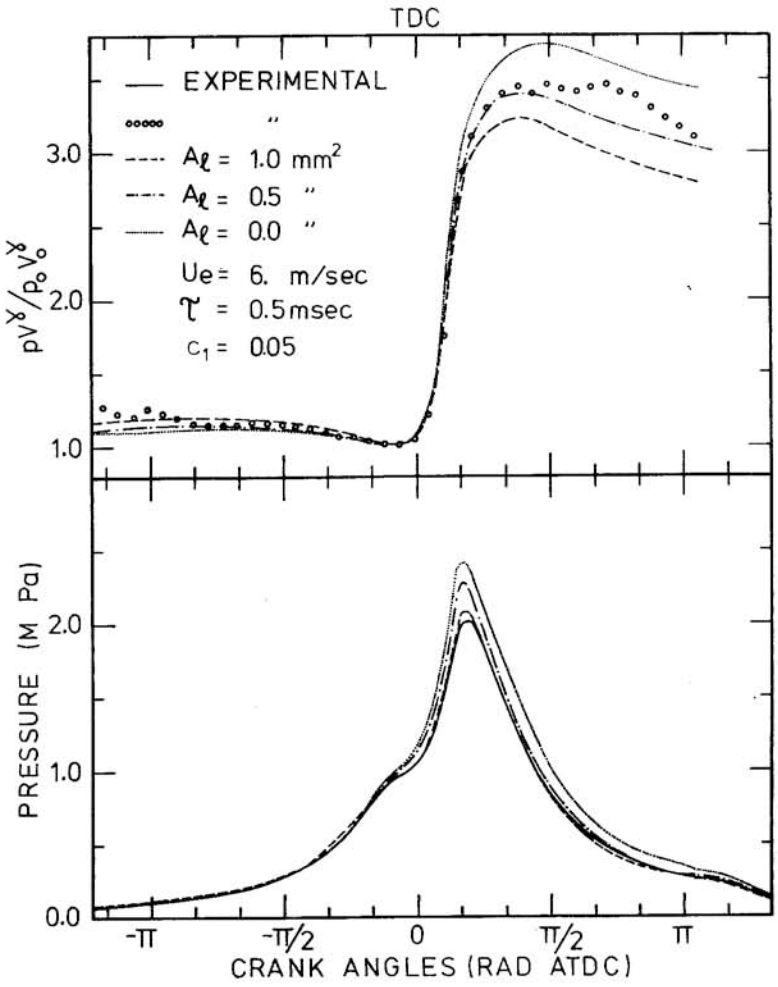

Fig. 14 - Effect of leakage area on pV^γ and pressure, during firing conditions holding other parameters constant

B. ENTRAINMENT SPEED AND BURNING TIME - In applying the model to predict engine performance at operating conditions different from the base condition, it was assumed that the leakage area A_ℓ and heat transfer correlation constant c_1 would remain unchanged. However, a decision had to be made about the way entrainment speed and the laminar burning time should scale with engine operating conditions. As a first approach it was decided that the entrainment speed u_e should scale lineraly with engine speed, and the characteristic burning time τ was then adjusted to fit the pressure vs. crank angle data. The values of u_e and τ used are given in Table 6. Also shown are values of τ computed from the relation

$$\tau = \tau_{ref}(S_{uref}/S_u) \qquad (26)$$

which assumes a constant characteristic eddy size. The reference condition was Run Number 9 and the laminar flame speed S_u was evaluated at the average unburned mixture temperature and pressure during combustion.

Table 6 - Entrainment Speed and Characteristic Laminar Burning Time

Run	u_e m/sec	τ msec.	τ* msec.
8	6	.28	.28
9	6	.5	.5
10	6	.92	.92
11	6	.5	.81
12	6	.5	.71
13	1.75	4.	1.04
14	12	.5	.5

* computed from equation 26

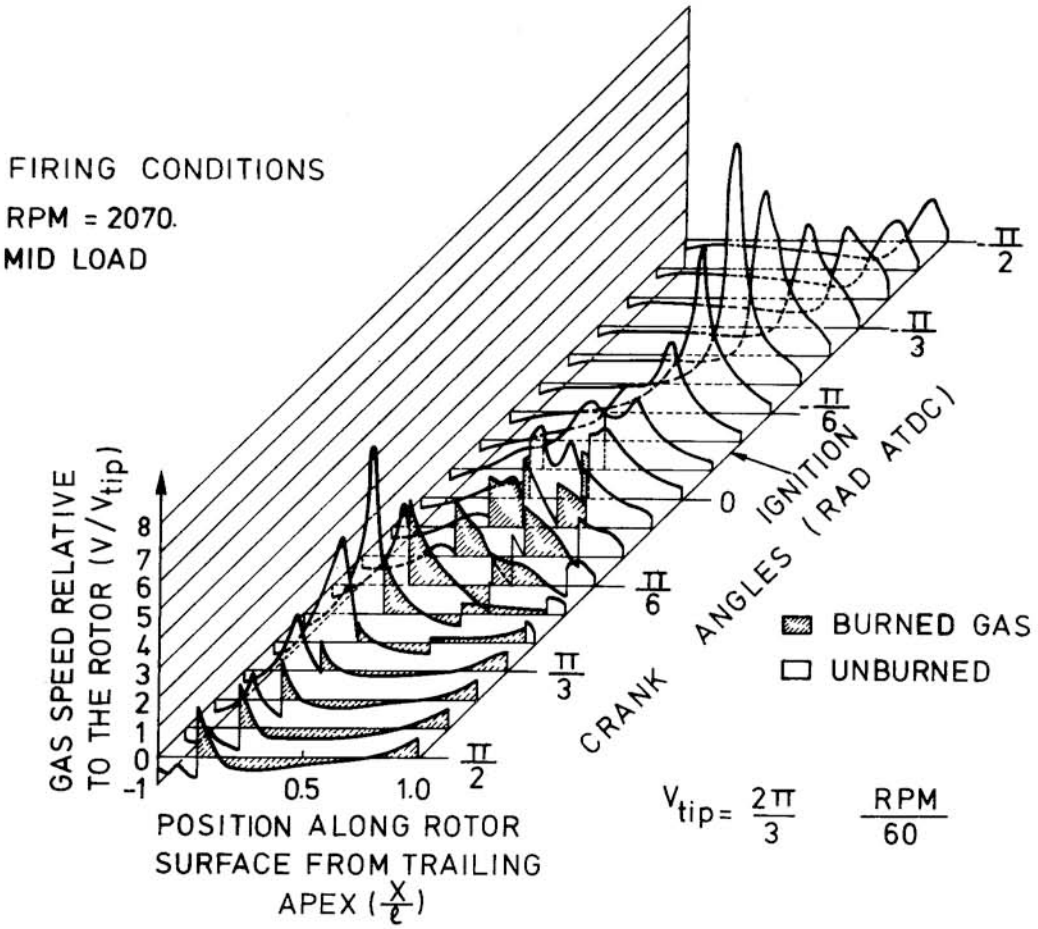

Fig. 15 - Gas motion induced by the changing chamber geometry and flame presence, relative to the rotor. Positive in the direction of rotation, nondimensionalized by the average rotor tip velocity

C. GAS VELOCITIES AND HEAT TRANSFER - Having fixed the values for the different parameters in the model, let us now examine what is happening inside the chamber while the engine is rotating. Figure 15 shows the gas velocity inside the chamber under the firing conditions: the cross-hatched part of the diagram represents the velocity of the burned gases, while the blank part refers to unburned gases. As can be seen there is a jump in gas speed at the point of separation between unburned and burned gas. This is due to rapid expansion of the burned gases due to heating. The corresponding heat transfer is shown in Figure 16. Notice that, although the velocities are lower in the burned gas than in the unburned gas, the heat transfer is larger due to the high value of the burned gas temperature.

D. HYDROCARBON EMISSIONS - Since the model includes both quenching and leakage, an attempt was make to compare measured average hydrocarbon concentrations with model predictions. It was assumed that, at each instant of time, the gas leaving a chamber had the average composition of the gas in the chamber. Since the composition and exhaust flow rate of this gas is known from the model, the unburned mass fraction in the exhaust gases is given by

$$x_{ue} = \int_{eo}^{ec} \dot{m}\, x_u\, dt \Big/ \int_{eo}^{eo} \dot{m}\, dt \qquad (27)$$

where x_u is the unburned fraction of the gases inside the chamber and eo and ec indicate values at exhaust port open and close. The hydrocarbon concentration in ppm carbon for isooctane/air mixtures is then given by:

$$(HC) = \frac{8\ MW_e}{114}\, x_{ue}\, (1 - r_f)\, \frac{\Phi}{15.1 + \Phi}\, 10^6 \qquad (28)$$

where r_f is the residual fraction, MW_e is the average molecular weight of the exhaust gases and Φ is the fuel-air equivalence ratio of the unburned charge. The results of this computation are displayed in Table 7 where a distinction is made between quenching and leakage generated

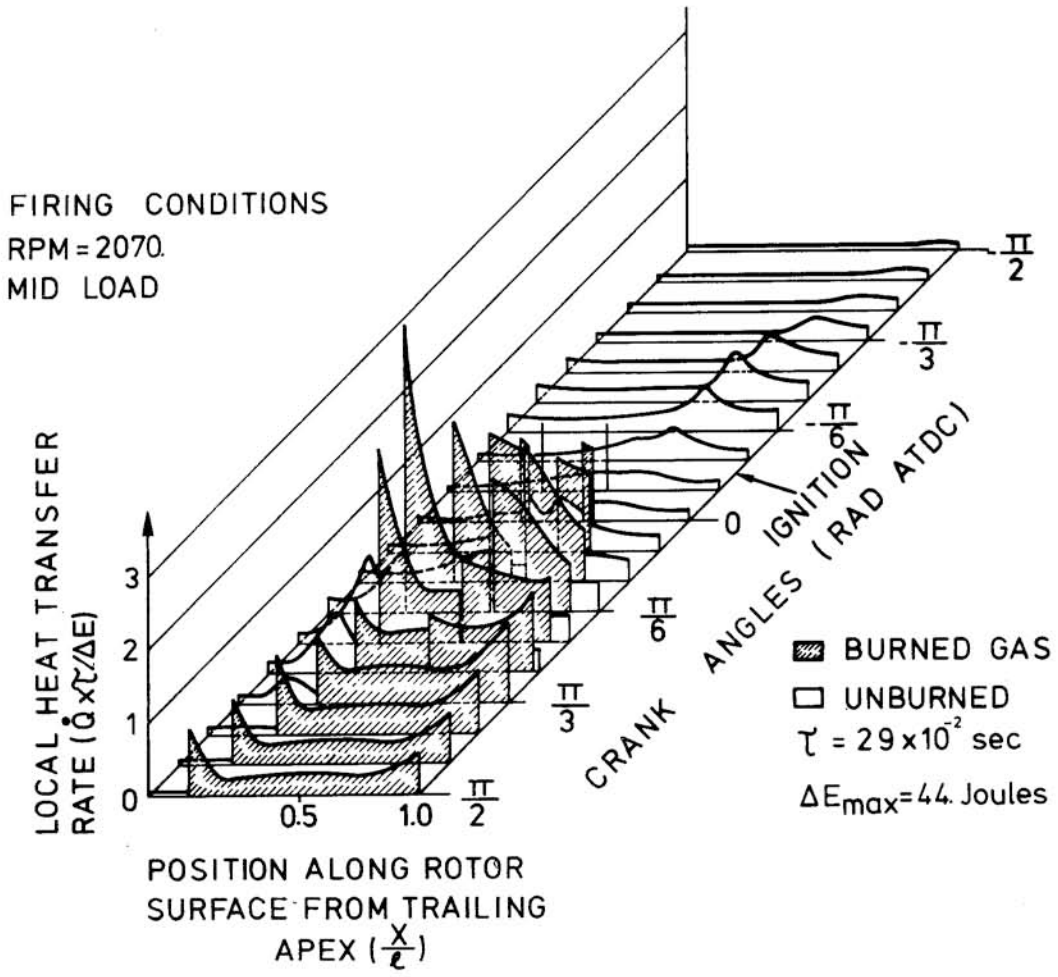

Fig. 16 - Heat transfer due to the gas motion, versus crank angle and position along the rotor surface. Nondimensionalized by the heat of combustion of the fuel (ΔE), and the period of one crank shaft rotation (τ)

hydrocarbons. The error between experimental and theoretical values is shown, together with fuel-air equivalence ratios and the measured exhaust temperature.

The overall levels predicted are comparable with measurements (and are higher as would be expected since oxidation is omitted from the model). Quench and leakage are approximately equal as HC sources. The worst discrepancy occurs on the richest run.

Consider first the quench HC for the 2000 RPM cases: Runs 8,9,10,11 and 12. Run 8 is a wide-open throttle case with the highest pressures and temperatures, Run 9 is partly throttled and Run 10 is fully throttled; these are characterized by successively lower temperatures and pressures (fuel-air ratios are stoichoimetric) and the quenched fraction increases as expected. Runs 11 and 12 show the expected effect of increasing quench fractions for mixtures leaner and richer than stoichiometric.

Leakage hydrocarbons are almost constant at constant speed (Runs 9-12) and are about 6% of the intake mass. When the speed is halved

Table 7 - Measured vs. Predicted Hydrocarbon Concentration

Run	$[HC_{meas}]$	$[HC_{pred}]$	x_q [a]	x_ℓ [b]	error [c]	ϕ [d]	T_e [e]
	ppm C		%	%	%		Deg. K
8	7000	7100	2.4	3.8	1	1.04	839
9	8400	8800	4.1	4.7	5	1.02	938
10	9400	11700	5.8	6.4	25	.99	898
11	9500	15500	7.0	5.4	63	1.26	923
12	8100	9200	5.9	4.9	14	.85	953
13	16200	20300	8.3	11.1	25	1.05	718
14	5400	7500	4.0	2.6	39	1.08	1023

a x_q = fraction of unburned gas due to quenching
b x_ℓ = " " " " " " leakage
c error = $([HC]_{pred} - [HC]_{meas}) / [HC]_{meas} \times 100$
d ϕ = equivalence ratio (fuel-air ratio/stoichiometric fuel-air ratio)
e T_e = exhaust temeprature

(Run 13) the leakage contribution doubles; when the speed doubles (Run 14) the leakage contribution halves. Finally, Run 8 has the lowest leakage at 2000 RPM, but due to the advanced ignition timing, the mass on the leading side of the chamber burned completely in a short time reducing the unburned gas leaked into the exhausting chamber.

To conclude, the hydrocarbon production model seems in reasonable agreement with experimental measurements which supports the validity of our models for quenching and leakage. More work is needed, however, on oxidation and vortex roll up to match time-resolved hodrocarbon measurements (23).

PARAMETRIC STUDIES OF ENGINE PERFORMANCE

Two parametric studies were done to see what improvement could be obtained by leakage or heat transfer reduction. While leakage can be reduced by improved seal design, reductions in heat transfer can only be obtained through changing the material of the housing (e.g. by using steel instead of aluminum, or even ceramics) or changing the geometrical shape of the chamber.

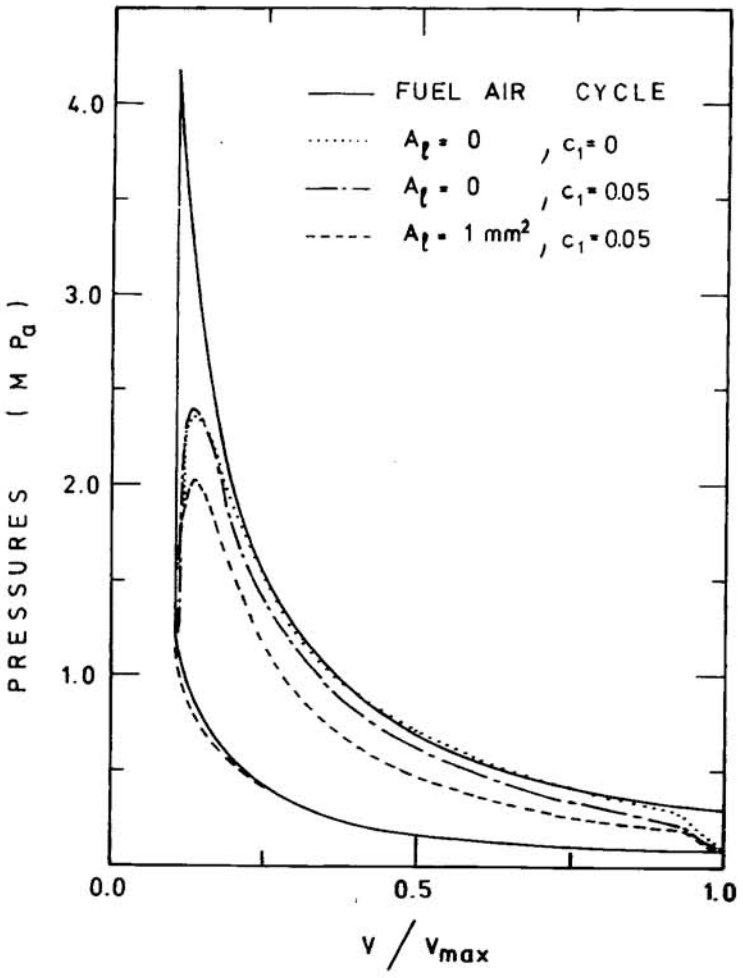

Fig. 17 - Comparison between fuel-air cycle, adiabatic real cycle, and cycles with heat transfer and leakage

The model was first run with both zero heat transfer and leakage area. Then heat transfer was included with leakage kept to zero. Finally both heat transfer and leakage were included. Runs were made holding the intake plenum pressure and ignition timing constant. The results of this simulation are displayed in Figure 17 on a p vs. V plot, on which the fuel-air cycle corresponding to the adiabatic case is also shown. Note that, after the end of the combustion and all during expansion, the model predicts values of pressure for the real adiabatic cycle case which are larger than the fuel-air values.

Table 8 presents the indicated thermal efficiencies of each of the simulations. As can be seen a big improvement in efficiency could be obtained if leakage were drastically reduced (actually, in the case of the engine tested (case 0), the real efficiency was even lower (22 instead of 26%) due to the previously mentioned mismatch of the intake masses). We should however, remember that leakage is a strong function of speed (this was a low speed run - 2000 RPM) and leakage was probably increased by holes in the housing necessary for inserting the pressure transducers. Hence standard engines could have better performances than the one tested here.

The conclusions that can be drawn on the basis of the present analysis are similar to those previously obtained by Danieli et al (24) The biggest loss relative to the fuel-air cycle is due to the finite combustion speed. Next comes heat transfer, and even a small decrease would be beneficial for engine performance. Leakage appears to be a smaller problem though improvements are especially important at low speed.

Note that in the previous work (24), simulations were made holding the brake output constant. Hence the estimates of the efficiency gains to be obtained from leakage or heat transfer reduction differ, the new ones being larger. The efficiency improvements attainable through leakage reduction are consistant with those of Eberle and Klomp (2).

Table 8 - Indicated Efficiency Gains from Heat Transfer Reduction

Case	A	c_1	η	$\frac{\eta - \eta_o}{\eta}$
	mm^2		%	%
0	1.0	0.05	26.0	0
1	0.5	0.05	28.2	8.5
2	0	0.05	30.3	16.5
3	0	0.0	36.2	39.2
4	Fuel Air Cycle		42.5	63.6

CONCLUSIONS

A computer simulation of the Wankel engine operating cycle has been developed. Given the engine geometry, speed, equivalence ratio and inlet manifold conditions, the simulation predicts mass flows of fuel and air, chamber pressure, unburned and burned gas temperatures, heat transfer, gas leakage and quenching throughout the operating cycle. From these variables, engine power, efficiency, average heat transfer, leakage and hydrocarbon emissions are computed.

The basis of the simulation is the analysis of each chamber in the engine as a separate thermodynamic system, connected via the apex seal leakage path. By dividing each system into zones, gas motion induced by geometry changes as the rotor rotates, are calculated. From the velocity distribution, the instantaneous heat flux to the rotor and housing is computed using pipe flow convective heat transfer correlations. Gas leakage paths are combined as an effective leakage area at each apex seal. A turbulent entrainment combustion model is used to predict the flame front motion and burn-up rate behind the flame; combustion can be initiated at two spark plug locations. A wall quench model computes hydrocarbon production during combustion with unburned gas leakage to the exhausting chamber. This provides a basis for estimating HC emissions.

Values of the effective leakage area and the coefficient in the convective heat transfer correlation were determined by matching predicted chamber pressures to measured pressure curves under both motoring and firing conditions. During motoring, independent values for these parameters were determined by using the different speed dependence displayed by the two phenomena. During firing, the matching was done for one set of engine conditions. The leakage area (1 mm^2 per apex seal) so determined was smaller than the value determined from motoring conditions (1.5 mm^2). The heat transfer correlation coefficient $c_1 = 0.05$ determined by this process was 1.5 times the value used in reciprocating engines heat transfer correlations (6).

With parameters chosen to match one set of experimental conditions, predictions of chamber pressure at other engine operating conditions were in reasonable agreement with the data. The predicted mass flow rates were lower than the measured mass flow rates. The omission of mass loss between intake and exhaust, via side seal leakage, is believed to be one significant factor contributing to this discrepancy.

Parametric studies of the effects of leakage and heat transfer reductions on engine efficiency show these loss mechanisms to be comparable in magnitude (with heat transfer the larger) A ten percent reduction in leakage and heat transfer would improve specific fuel consumption by 1.7 and 2 percent respectively (at 2000 RPM, mid-load conditions).

LIST OF SYMBOLS

A_f	flame front surface
A_ℓ	effective leakage area per apex seal
c_d	discharge coefficient
c_1	heat transfer correlation coefficient
c_2	quenching correlation coefficient
E	total energy of the system
e	specific energy of the system
f	function of variables between parentheses
H	total enthalpy of the system
h	specific enthalpy of the system
ℓ	characteristic length
ℓ_e	characteristic laminar burning scale
m	mass
MW	molecular weight
Nu	Nusselt number
p	pressure
Pe	Peclet number
Q, Q_{loss}	heat loss
R	specific gas constant
Re	Reynolds number
S_u	laminar burning speed
T	absolute temperature
t,t'	time
u	gas speed
u'	turbulent fluctuating velocity
V	volume
W, W_{usef}	work output
x	mass fraction
α	thermal diffusivity
γ	ratio between specific heat at constant pressure and specific heat at constant volume
δ	thickness
ε	energy dissipation rate
ρ	density
τ	characteristic time
Φ	equivalence ratio

SUBSCRIPTS

ave	average
b	burned products
d	displacement
e	entrained
ec	exhaust close
eo	exhaust open
exh	exhaust
f	flame front
fir	firing conditions
flow	flow measurements
front	front rotor
HC	associated with hydrocarbon
i	i^{th} subsystem
in	entering flux
int	intake
j	j^{th} subsystem
jk	fluxes from the j^{th} to the k^{th} subsystem
k	k^{th} subsystem
l	leading apex
ℓ	leakage
mot	motoring distance
out	flux in exit
rear	rear rotor
ref	reference
t	trailing apex
TH	thermodynamic
u	unburned mixture
unb	unburned mixture due to incomplete combustion

SUPERSCRIPTS

-	average of the quantity
	time rate of the quantity

ACKNOWLEDGMENTS

The authors wish to express their gratitude to Dr. Kenichi Yamamoto of Toyo Kogyo Co. Ltd., Dr. Charles Jones and Mr. Vincent Pohlmeyer of Curtiss Wright Corp., Dr. David P. Hoult and Prof. Borivoje B. Mikic of M.I.T. The engine was provided by Curtiss Wright and the work supported by the Ford Professorship of Dr. James C. Keck.

REFERENCES

1. F.V. Bracco and W.A. Sirignano, "Theoretical Analysis of Wankel Engine Combustion," Combustion Science and Technology, Vol. 7, (1973) pp.109-123.
2. M.K. Eberle and E.D. Klomp, "An Evaluation of the Potential Performance Gain from Leakage Reduction in Rotary Engines," SAE Trans., Vol. 82, paper 730117 (1973).
3. G.A. Danieli, C.R. Ferguson, J.B. Heywood and J.C. Keck, "Predicting the Emissions and Performance Characteristic of a Wankel Engine," SAE Trans., Vol. 83, paper 7400186 (1974)
4. N.C. Blizard and J.C. Keck, "Experimental and Theoretical Investigation of Turbulent Burning Model for Internal Combustion Engines," SAE Trans., Vol. 83, paper 740191 (1974).
5. E. Eichelberg, "Some New Investigation on Old Combustion Engine Problems," Engineering, Vol. 148 (1939)
6. G. Woschni, "A Universally Applicable Equation for Instantaneous Heat Transfer Coefficient in the Internal Combustion Engine," SAE Trans., Vol. 76, paper 670931 (1967)
7. W.M. Rohsenow and H.Y. Choi, "Heat, Mass and Momentum Transfer," Prentice Hall,Englewood Cliffs, 1961.
8. C.R. Ferguson and J.C. Keck, "On Laminar Flame Quenching and its Applications in Engine Combustion," Comb. & Flame,28,197 (1977)
9. R.F. Ansdale, "The Wankel RC Engine", Iliffe London, 1968.
10. G.A. Danieli, "A Performance Model of a Wankel Engine, Including the Effects of Burning Rates, Heat Transfer, Leakage and Quenching Compared with Measured Pressure Time Histories," Ph,D. Thesis, Dept. of Mech. Eng., M.I.T. January 1976.
11. M.K. Martin and J.B. Heywood, "Approximate Relationships for the Thermodynamic Properties of Hydrocarbon-Air Combustion Products," Combustion Science and Technology, Vol. 15, pp. 1-10, 1977
12. S.D. Hires, A. Ekchian, J.B. Heywood, R.J. Tabaczynsky, J.C. Wall, "Performance and NO_x Emissions Modelling of a Jet Ignition Prechamber Stratified Charge Engine," SAE paper 760161, 1976
13. F.T. Krogh, "A Variable Step Variable Order Multilisted Method for the Numerical Solution of Ordinary Differential Equations," Information Processing 1968: Proceedings of IFIP Congress 1968 (A.J.H. Morrel, Editor), Vol. 1, pp. 194-199, North Holland Publishing Company, Amsterdam, 1969
14. G.A. Danieli, J.C. Keck and J.B. Heywood, "Experimental and Theoretical Investigation on Motoring Performances of a Wankel Engine," Atti del Dipartimento, Dip, di Meccanica, Universita della Calabria, n° 5, gennaio 1977.
15. G.A. Danieli, J.C. Keck and J.b. Heywood, "Experimental and Theoretical Investigation on Firing Performances of a Wankel Engine," Atti del Dipartimento di Meccanica dell' Universita della Calabria, n° 7, febbraio 1977.

16. R.E. Windsor and D.J. Patterson, "Mixture Turbulence - A Key to Cyclic Combustion Variation," SAE Trans., Vol. 82, paper 730086, (1973)
17. K. Yamamoto, "Rotary Engine," Toyo Kogyo Co., Ltd., Hiroshima, 1969.
18. R. Friedman and W.C. Johnston, "The Wall-Quenching of Laminar Propane Flames as a Function of Pressure, Temperature, and Air-Fuel Ratio," Jol. Applied Physics, Vol. 21 (1950).
19. A.H. Shapiro, "The Dynamics and Thermodynamics of Compressible Fluid Flow," The Ronald Press Co., New York, 1953.
20. D.R. Lancaster, R.B. Kreger, and J.H. Lenesch, "Measurement and Analysis of Engine Pressure Data," SAE Trans., Vol. 84, paper 750026, (1975)
21. R.S. Spindt, "Air-Fuel Ratios from Exhaust Gas Analysis," SAE Trans., Vol 74, paper 650507, (1965)
22. K. Yamamoto and T. Kuroda, "Toyo Kogyo's Research and Development on Major Rotary Engine Problems," SAE Trans., Vol. 79, paper 700079, (1970)
23. C.R. Ferguson, G.A. Danieli, J.B. Heywood and J.C. Keck, "Time Resolved Measurements of Exhaust Composition and Flow Rate in a Wankel Engine," SAE Trans, Vol. 84, paper 750024, (1975).
24. G.A. Danieli, C.R. Ferguson, J.B. Heywood, and J.C. Keck, "Analysis of Performance Losses in a Wankel Engine," Conference on Combustion in Engines, Institute of Mechanical Engineers, July 1975, Cranfield Institute of Technology

Society of Automotive Engineers, Inc.
400 COMMONWEALTH DRIVE, WARRENDALE, PA. 15096

24 page booklet. Printed in U.S.A.